VOLCANIC IMPACTS IN GRANULAR MEDIA

A Dissertation
Presented to
The Academic Faculty

By

Julian Spencer McAdams

In Partial Fulfillment
of the Requirements for the Degree
Masters of Science in the
School of Earth and Atmospheric Sciences

Georgia Institute of Technology

December 2017

VOLCANIC IMPACTS IN GRANULAR MEDIA

Approved by:

Dr. Dufek, Josef
School of Earth and Atmospheric Science
Georgia Institute of Technology

Dr. Newman, Andrew
School of Earth and Atmospheric Science
Georgia Institute of Technology

Dr. Ferrier, Kenneth
School of Earth and Atmospheric Science
Georgia Institute of Technology

Date Approved: December 1st , 2017

ACKNOWLEDGEMENTS

I would like to thank:

Josef Dufek for his assistance and guidance these last 5 years as an employee and 2.5 as a student.

My committee: Josef Dufek, Andrew Newman, and Ken Ferrier.

The Dufek Group: Mary Benage, Jenn Telling, Ozge Karakas, Joe Estep, Joshua Méndez, Andrew Gase, Ryan Cahalan, Amelia Winner, Will Guinn, Gabe Eggers, Brenna Halverson, Dylan Casler, Eric Breard, and James Cowlyn.

Other mentors: From the GT machine shop: Steven Sheffield, Scott Elliot, Louis Boulanger, Nathan Mauldin, Frank Murdock, and Matt Carroll and the GT Clean room: Eric Woods.

Student assistants: Andrew Gase, Kelly Flanagan, Katie Gardner, and Will Guinn for their assistance in experiments.

My mother, Lisa, and grandparents, Nancy and Spencer, for their continued support throughout my entire career at Georgia Tech.

The Reese family: Keith, Angela, and Adam.

Most of all my beautiful and supporting wife Mary McAdams who is by my side through late nights and early mornings and always there to bring a smile to my face.

TABLE OF CONTENTS

AKNOWLEDGEMENTS **iii**

LIST OF TABLES **v**

LIST OF FIGURES **vi**

LIST OF SYMBOLS AND ABBREVIATIONS **viii**

SUMMARY **ix**

CHAPTER 1. VOLCANIC IMPACTORS AND CRATER FEATURES **1**
1.1 Introduction 1
1.2 Phreatic Eruptions 2
1.2.1 Maars 2
1.3 Pyroclasts 3
1.4 Bomb sags 4
1.5 Previous works 8

CHAPTER 2. VOLCANIC IMPACT EXPERIMENTS **9**
2.1 Goals in this work 9
2.2 Experimental design 9
2.3 Methods 10
2.4 Data 12
2.5 Discussion 17

CHAPTER 3. FUTURE WORK **21**
3.1 Goals in future work 21

APPENDIX RAW DATA **23**

REFERENCES **26**

LIST OF TABLES

Table 1 - Impactor properties 10

Table 2 - Substrate grain sizes 11

Table 3 - Graph key for figures 9 and 10 13

Table 4 - Scaling factors for McAdams model 14

Table 5 - Scaling factors for equations 2 and 3 for Birch et al. models 19

Table 6 - Graph key for figures 20 through 25 23

LIST OF FIGURES

Figure 1 - The make-up of phreatic maars (USGS) shows a diatreme approaching a crater lake resulting in a phreatic eruption 2

Figure 2 - Atexcac crater, Serdán-Oriental Volcanic basin, Mexico image by author 3

Figure 3 - Ubehebe crater, Death Valley, California image by author 3

Figure 4 - Bomb sag feature at Ubehebe crater with author 5

Figure 5 - Labeled bomb sag diagram 6

Figure 6 - A saturated impact. The red circle represents the ejecta diameter whereas the green circle is the crater diameter 7

Figure 7 - Air cannon apparatus with components labeled 10

Figure 8 - SEM images of Ballotini glass beads. From left to right coarse, medium, and fine glass beads at 603 times magnification 12

Figure 9 - The velocity to crater diameter relationship of the data. Note the clear separation of saturated and dry impacts with the dry impacts reaching larger crater diameters at lower velocities. 13

Figure 10 - The velocity to penetration depth relationship of the data. Note the influence of the impactor density and size on the penetration depth. 14

Figure 11 - McAdams model of saturated media impacts without scaling factors 15

Figure 12 - McAdams model of saturated media impacts with only γ, the impactor density parameter, applied. 15

Figure 13 - McAdams model of saturated media impacts with only β, the grain size parameter, applied. 16

Figure 14 - McAdams model of saturated media impacts with all scaling factors applied. 16

Figure 15 - McAdams model of saturated media impacts with the addition of the dry impact data set. 17

Figure 16 - Birch et al. model using the tangent of the angle of repose of the substrate parameter, μ. 19

Figure 17 - Birch et al. model using the grain size of the substrate parameter, δ. 20

Figure 18 - Rheometer cup with angled and flat inserts. 21

Figure 19 - A method for measuring the angle of repose of dry substrates. 22

Figure 20 - Velocity with crater diameter relationship for the coarse grain substrate. 23

Figure 21 - Velocity with crater diameter relationship for the medium grain substrate. 23

Figure 22 - Velocity with crater diameter relationship for the fine grain substrate. 24

Figure 23 - Velocity with penetration depth relationship for the coarse grain substrate. 24

Figure 24 - Velocity with penetration depth relationship for the medium grain substrate. 25

Figure 25 - Velocity with penetration depth relationship for the fine grain substrate. 25

LIST OF SYMBOLS AND ABBREVIATIONS

Δ	Angle of repose
μ	Tangent of angle of repose
A	Projected area of impactor (m^2)
d	Total depth of penetration of impactor (mm)
D_i	Diameter of impactor (m)
M_i	Mass of impactor (kg)
R_i	Radius of impactor (m)
U_i	Velocity of impactor (m/s)
V_i	Volume of impactor (m^3)
V_{Ti}	Terminal velocity of impactor (m/s)
ρ_i	Density of impactor (kg/m^3)
C_r	Crater radius (mm)
D_c	Diameter of crater (mm)
I_f	Impact force (N)
KE	Kinetic energy (J)
δ	Substrate grain diameter, average (m)
ρ_s	Density of substrate (kg/m^3)
ρ_{sg}	Density of substrate grains (kg/m^3)
Cd	Variable drag coefficient
g	Acceleration of gravity (m/s^2)
K_v	Kinematic viscosity of air at 20°C (m^2/s) = 15.11E-6
Re	Reynold's number (dimensionless)
ρ_a	Density of air at 20°C (kg/m^3)
α	scaling factor for degree of saturation
β	scaling factor for grain size
γ	scaling factor for impactor diameter
φ_f	Void fraction of substrate (unit-less) (used single stagger)
C_1,C_2	Unit-less scaling coefficients
α_1,α_2	Unit-less scaling exponentials

SUMMARY

Phreatic eruptions occur when magma interacts with ground or surface water and creates a rapid expansion of steam. These eruptions have the potential to be amongst the most disastrous natural events due to their unpredictability and the large amounts of mass ejecta released on short timescales. Understanding the processes that occur during phreatomagmatic volcanic eruptions is key to decreasing risk of physical and cultural impact in areas of high human population density.

Impact craters originating from ballistically ejected lithics during phreatic eruptions regularly create sag-like features, known as "bomb sags", in the underlying strata. Previous studies have related size, depth, composition, and grain size of these bomb sags to atmospheric density during eruption, assuming the ballistic impacts occur at terminal velocity [Manga et al. 2012, Birch et al. 2014]. Furthermore, cohesion of the underlying strata is also key to understanding the observed bomb sag morphology, hence the need to decipher their impact dynamics.

Our goal is to establish a key relationship between velocity and depth of impact is established using crater diameter, grain size of substrate, and impactor size and density using experimental techniques. We measure the physical properties exhibiting before and after an impact in granular media.

We establish a parameter we title the Mc parameter which incorporate the variables previous listed. Using scaling factors based upon saturation of the substrate, average grain size of the substrate, and density of the impactor we show a trend of the Mc parameter with impact velocity.

CHAPTER 1. VOLCANIC IMPACTORS AND CRATER FEATURES

1.1 Introduction

The study of various types of ballistic impactors and their respective crater features are crucial to achieve an improved understanding of volcanic eruption strength, volume, overall mechanics, and gives insight into overpressure that develops throughout eruptions. Understanding the mechanics of these volcanic eruptions is key to grasp the extent of volcanic hazards and in some case prevent environmental and human loss. According to a recent volcanic fatalities database (Brown et al., 2017) over 29 million people worldwide live within just 10 km of active volcanoes, and around 800 million people live within 100 km. Therefore, it is essential for geophysical scientists to research numerous aspects of volcanism both in the field as well as testing by utilizing computational modeling mechanisms.

Aside from giving insight into eruptive processes, ballistic impactors are a hazard of their own. Of the 214,004 fatalities from all eruptive hazards in the study by Brown et al., 4682 perished from ejecta including tephra and ballistics. In many cases the observation of fallout extent and dispersal is used to model the eruptive conditions (Steinburg et al., 1977, Carey et al., 1986, Wilson et al., 1987, Bower et al., 1995, and Mastin et al., 2001). The focus of this study is to better understand impact velocities of volcanic bomb impacts in both dry and saturated substrates. By constraining the impact velocities of these various bombs we can increase the resolution of eruptive models and atmospheric condition models.

1.2 Phreatic Eruptions

Ballistic impactors are generated through various eruptive settings. As a result of the tremendous overpressures developed by the rapid expansion of water to steam, eruptions that contain a phreatic component often form large ballistic particles. These eruptions are produced when heat of magma comes into contact with ground or surface water to drive the expansion of steam (figure 1). An example of phreatic eruptions are the many steam explosions that preceded the 1980 Plinian eruption of Mount St. Helens. If molten magma comes in direct contact of the water source, it is classified as a phreatomagmatic eruption and contains juvenile clasts. These eruptions occasionally create broad, low-relief craters called maars.

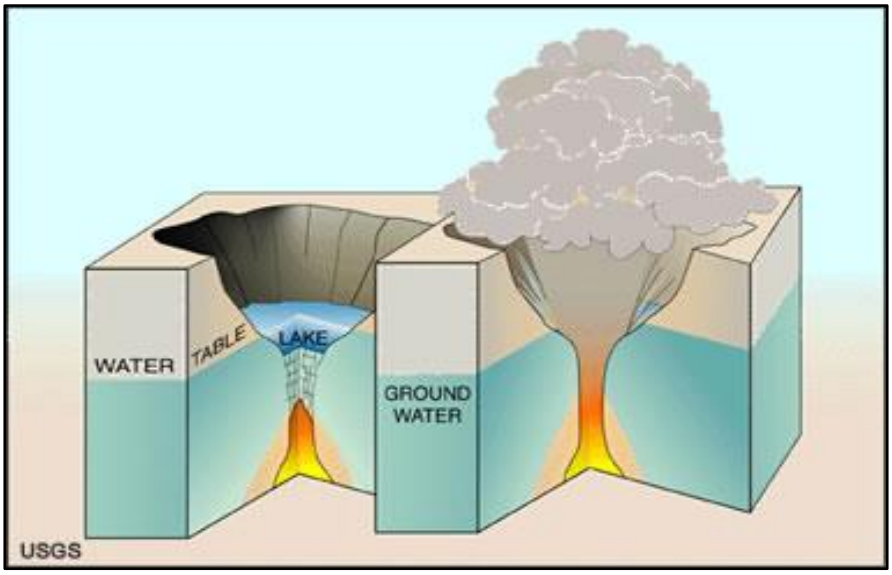

Figure 1- The makeup of phreatic maars (USGS)

1.2.1 Maars

Maars are shallow, flat basin craters. Many form maar lakes such as Aljojuca, Atexcac (figure 2), and Alchichic maars in the Serdan-Oriental Volcanic Basin in Mexico (Carrasco-Núñez et al.,2006). Maars can also have dry basins, which are called

xalapazcos in Mexico. A key example of a dry maar is Ubehebe crater in Death Valley, California (figure 3).

Figure 2- Atexcac crater, Serdan-Oriental Volcanic Basin, Mexico

Figure 3- Ubehebe crater in Death Valley, California

During the eruptive sequence of a maar, overlying rock, steam, water, ash, and in some cases juvenile magmatic material are ejected. This material falls to the surrounding crater and if lithified forms a matrix of ash and lithics known as a tuff ring. As a result of the wet nature of maar formation from phreatic eruptions the fallout is often saturated. A saturated ash and tephra layer create cohesive conditions of the substrate. Contrary to impacts in dry and non-compacted strata, lithics impacting saturated strata create substantially less ejecta.

1.3 Pyroclasts

Pyroclasts are ejected material, either from the overlying rock or from magmatic sources, which can drastically vary in vesicularity and size based upon genesis. These

clasts vary in size from fine ash (<750 microns) to blocks and bombs (>64mm) (Schmid, 1981). Once deposited, pyroclasts are referred to as tephra. Deposition of these clasts occur through the three main volcanic modes of transport, flow, surge, and fall.

A pyroclastic flow is a mixture of heated gas and pyroclastic material, propelled by gravity and buoyant forcing, that create high concentration deposits of tephra (Sparks et al., 1982). If a flow has a higher proportion of gas than rock it is often referred to as a surge. Surges occur both independently as well as intertwined with pyroclastic flows, and hence the term pyroclastic density current (PDC) is now generally used to refer to the continuum of currents between surges and flows. Surges have much lower densities than flows and can therefore detach from and travel further than their parent flows (Calder et al., 1999).

Pyroclastic falls consists of material that is ejected from an eruption and descend as either ballistics, ash and lapilli settling from convective clouds existing in flows, or from the plume itself. Wind patterns can shift the trajectory of these falls anywhere from a few hundred meters to over 2.8 kilometers (Walker et al., 1971). Often the sedimented impacts of bombs and blocks and deposition of ash and lapilli are used to track the pyroclastic fallout such as the case for the 1989-1990 Redoubt eruptive sequences (Scott et al., 1991). In this work we focus mainly on pyroclastic falls, specifically bombs and their impact features.

1.4 Bomb Sags

Bomb sags are formed from ballistically ejected lithics during phreatic eruptions (Manga et al., 2012). These lithics form a sag-like feature in the underlying strata due to the cohesion of grains from water sourced from the eruption. Without cohesion, from

either water or electrostatic forcing, impacts are unable to form bomb sags and instead create ejecta and mixing of the underlying strata as depicted by the experiments conducted in Manga et al., (2012). The degree of saturation and cohesion is dependent upon the packing regime of a granular bed. In natural cases a packing regime is extremely difficult to ascertain. In order to accurately represent the style of packing one must obtain an unaltered cross section of the granular bed (figure 4).

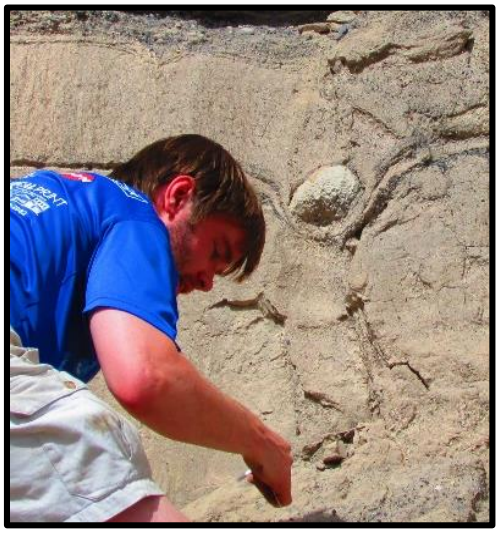

Figure 4-Bomb sag feature at Ubehebe crater with author

Impact features can be used to help determine the strength of a volcanic eruption, impact velocities, and the atmospheric density during eruption. In this work we arrive at a model for impact energies using measurements taken from bomb sags preserved in outcrops found in nature. These measurements include the density of the impactor and substrate, the average grain diameter of the substrate layer, the impactor diameter, the depth of penetration, and the crater diameter (figure 5). These physical components can help constrain what factors contribute to the aspect ratio of an impact crater, the velocity of an impactor at impact, and the effect of substrate grain size on impacts.

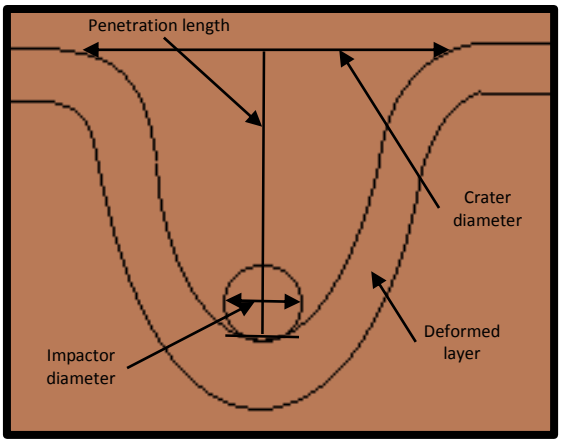

Figure 5-Bomb sag diagram

Bombs are defined by their shape and morphology which is determined by the gaseous composition and viscosity of the source magma (Walker et al., 1971). There are several sub classifications of pyroclastic bombs including, breadcrust bombs, ribbon bombs, spindle bombs, and spheroidal bombs. Most bombs that form sag features are of higher density (Taddeucci et al., 2017) In this work we focus predominantly of spherical bombs.

Penetration depth is defined as the point at which the base of the clast settles in the underlying strata. The depth length is the distance from the initiation of the dipping layer to the penetration depth. The aspect ratio of the crater is the ratio of penetration depth to crater diameter. In the cases of saturated impacts there are two rings that develop post impact, one is the crater diameter and one is the ejecta ring which is much like a tuff ring from a maar (figure 6).

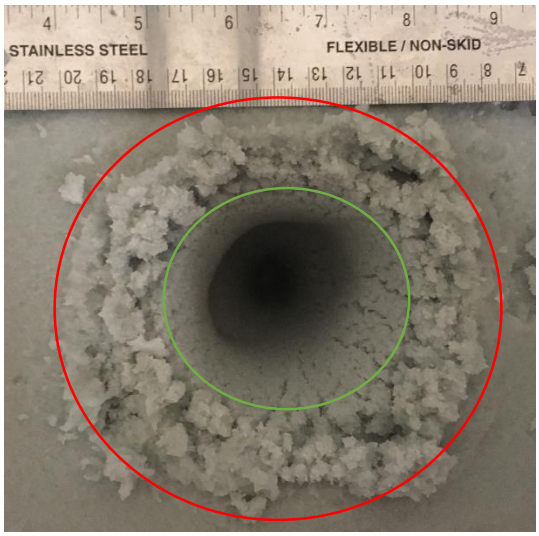

Figure 6- A Saturated impact. The red circle represents the ejecta diameter whereas the green circle is the crater diameter

Cohesion of the granular bed is also a necessary component and is produced predominantly due to water from the source eruption. The degree of saturation of the bed alters the morphology of the resultant impact crater. Over saturation (degree of saturation over 100%) is created when standing water exist on the surface of the grain and induces crater filling and erosion by the fluid, thus inhibiting the formation of sedimented sag layers. Under saturation (degree of saturation <25%) creates mixing, ejecta, but no sedimented sag layer. The ideal degree of saturation in this work was found to be between 50 and 100%, which produces a negative direct relationship between the slope of the crater wall and degree of saturation.

1.5 Previous works

Currently the most closely related studies that have developed a depth of penetration relation use low velocity impacts into dry, (Katsuragi et al., 2007), and saturated (Manga et al., 2012 and Birch et al., 2014) substrates and therefore are not applicable to this study. While these works described the general dynamics of these lower energy impacts, analysis of impact velocity (Taddeucci et al., 2017), and theoretical predictions (Mastin, 2001), both indicate energies outside the calibration range of these experiments. Here, we examine penetration depth of impactors across a broader energy range to better determine impact conditions in deposits.

CHAPTER 2. VOLCANIC IMPACT EXPERIMENTS

2.1 Goals in this work

Here, we strive to solve for velocity of impact into glass particle substrate by experimentation. Using the physical properties that can be established from a typical bomb sag feature in an outcrop we will create a simple numerical model that can back calculate the impact velocity. With this new information we may better constrain ballistic trajectories and atmospheric densities of eruptions long after the eruptive event. We may also better understand the necessary conditions for bomb sags to form.

2.2 Experimental design

Experiments are completed using a cannon constructed from steel and plastic components (Figure 7). The cannon functions using compressed air collected in an air collection chamber. A solenoid valve controls the flow of air from the air collection chamber to a quick exhaust valve. The air is rapidly discharged through the quick release connector and then through the cannon barrel thus propelling the impactor to the impacting bed below.

In order to ensure safety of the cannon operator the firing process is completed wirelessly. An Xbee antenna with a range of approximately 100 meters is connected to a computer with RealTerm serial/TCP terminal. A series of simple commands are sent to an Arduino Uno board connected to the cannon in order to fire an impactor. To achieve higher velocity impacts the air pressure is increase by use of an air regulator. The max air pressure allowed for the solenoid is 6.9 bars. This allows for maximum velocities of 130 m/s for the small spheres, 10.9-11.5 millimeters in diameter, and 80 m/s for the medium spheres, 22.0 - 22.2 millimeters in diameter.

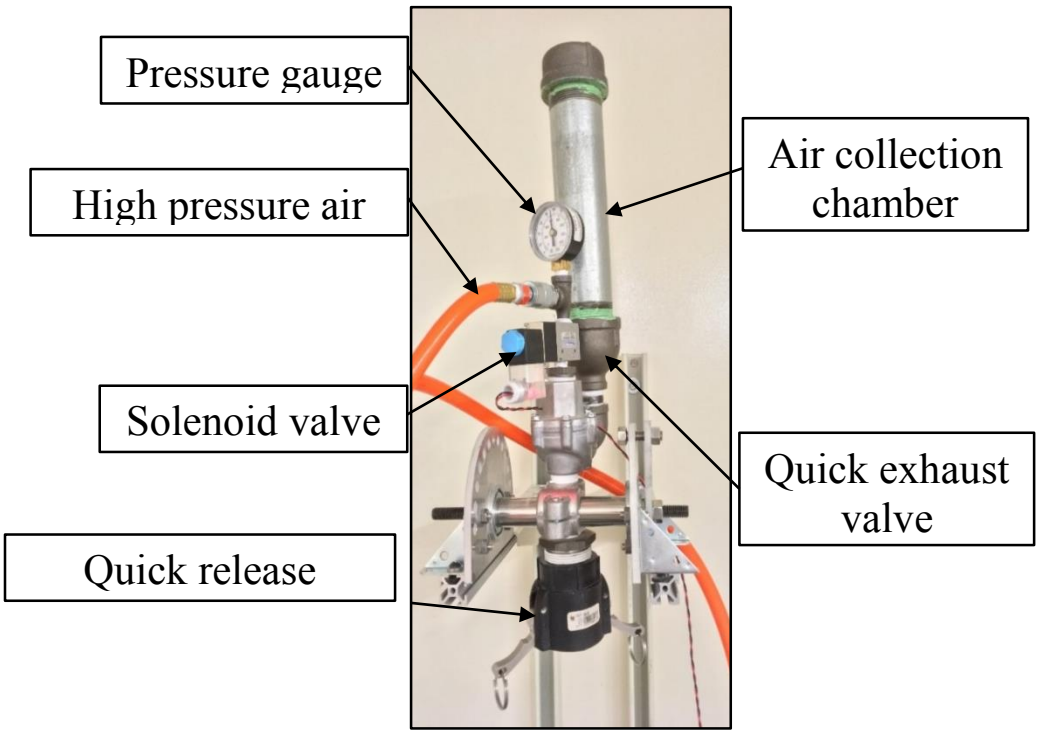

Figure 7- Air cannon apparatus

2.3 Methods

Spheres are two different sizes and varying densities are used. As a proxy to impactors found in nature, a glass impactor was used. In order to obtain a stark contrast a stainless steel impactor was also used. (Table 1)

Table 1-Impactor properties

IMPACTORS				
Material	**Mass (g)**	**Radius (cm)**	**Volume (cm^3)**	**Density (g/cm^3)**
Stainless Steel Medium	44.73	1.11	5.73	7.81
Green Marble Medium	13.89	1.10	5.57	2.49
Stainless Steel Small	8.20	0.58	0.80	10.30
Clear Marble Small	2.29	0.55	0.68	3.37

Velocity is measured using a Phantom Miro eX4 high speed camera. A ruler is initially placed within the firing path of the impactor in order to obtain a scale and removed prior to shot. The velocity is measured by noting the change in position of the impactor from frame to frame. In order to achieve the proper amount of exposure a 500W halogen work lamp illuminates the impactor shot path. Fringe affects occur on the impactor as velocity increases, therefore the pixel uncertainty in the high speed photos factors into the velocity uncertainty. The velocity is established at the base of the impactor across two images. The uncertainty is shown by evaluating the pixel difference from the base of the impactor to the base of the fringe effects.

Table 2

SUBSTRATE GRAIN SIZES	
Size D Ballotini: 212-300 microns	COARSE
Size AC Ballotini: 125-250 microns	MEDIUM
Size AE Ballotini: 90-150 microns	FINE

The impact bed is comprised of Ballotini glass beads. We use three size distributions shown by table 2 and figure 8. Shots are completed using both dry and saturated bed conditions. To achieve complete saturation, the bed is first over- saturated and mixed, allowed to settle overnight, and then the excess surface water is siphoned off. The bed is weighed before and after experiments to limit losses due to ejecta and evaporation.

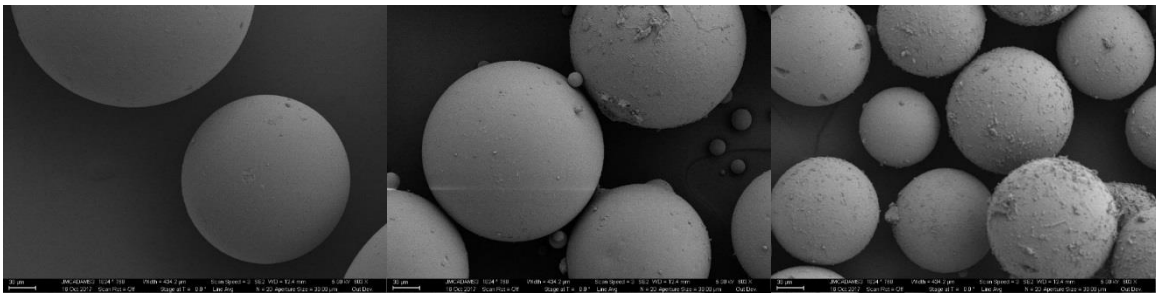

Figure 8- SEM images of Ballotini glass beads. From left to right coarse, medium, and fine glass beads at 603 times magnification

2.4 Data

In order to acquire a substantial data set 750 impactors were shot, 330 into a saturated substrate and 420 into a dry substrate. For each shot the impactor mass and diameter, the impact velocity, crater diameter, and penetration depth were recorded. The key relationships that were made include penetration depth and crater diameter based upon impact velocity varying with grain size, and a developed model with scaling that relates energy of impact to the observable properties of a bomb sag.

To provide a method for finding impact velocities from the observable sags a scaling analysis was performed. The density (ρ) of the impactor and substrate, average substrate grain size (δ), impactor radius (R_i), depth of penetration (d), and crater radius (C_r) are all factors used in Mc value. In order to condense the data into a more linear relationship on the log/log scale the equation is raised to the 1/6th power. A more extensive representation of the data set is shown in the appendix of this thesis.

$$Mc = \alpha\beta\gamma\left(\left(\frac{\rho_i}{\rho_s}\right)\left(\frac{\delta}{R_i g}\right)/\left(\frac{d}{C_r}\right)\right)^{\left(\frac{1}{6}\right)} \quad \text{(Eq 1)}$$

First, considering the cohesive forces created by a saturated substrate it is reasonable to hypothesize that grain bed saturation alters the morphology of an impact crater. From the experiments we find that the average crater diameters of dry substrate impacts are 2.95 times larger than those of impacts into saturated grain beds. This relationship is

shown in figure 9 for the medium grain size and the key for the following graphs is shown in table 3. The difference in crater diameters is clearly shown in this figure as well as the difference in max velocity of the less dense spheres which is due to the work needed by the air cannon to push denser impactor through the barrel.

Table 3-Graph key for figures 9 and 10

Saturated substrate	Solid circle markers with solid line
Dry substrate	Hollow diamond markers with dotted line
Medium Stainless Steel Sphere	Blue
Small Stainless Steel Sphere	Grey
Medium Marble Sphere	Orange
Small Marble Sphere	Green

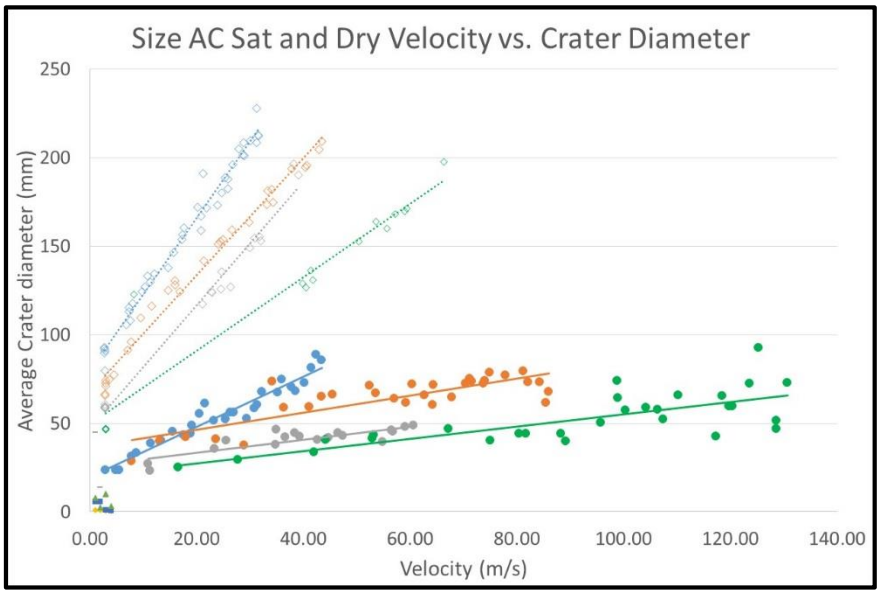

Figure 9

Second, the density of the impactor is the main factor that influences depth of penetration. It is shown in figure 10 that the larger diameter and denser impactor has the greatest depth of penetration. The penetration depths are also deeper in non-saturated impact beds because of the lower bed density without the addition of water in the void space.

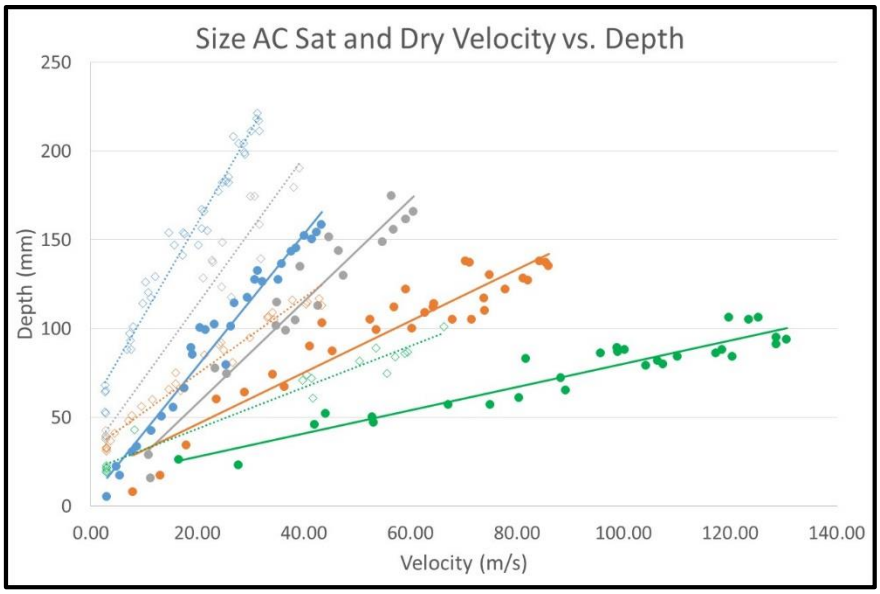

Figure 10

Finally, incorporating the entire data set we established 3 scaling factors shown in table 4. These factors were applied in the Mc number to scale the data set accordingly. The progression of the following 5 figures shows the effect of each scaling factor upon the total data set. Each graph is on a log/log scale.

Table 4

α	Dry	Scaling for level of saturation, if 0 the data will not be plotted
	Saturated	
β	AE	$\beta=(\delta-\delta_{avg})*\psi_1$ ψ_1 is set at 1E-3
	AC	
	Dry	
γ	SS Medium	$\gamma=(D_i-D_iavg)*\psi_2$ ψ_2 is set at 18
	SS Small	
	Marble Medium	
	Marble Small	

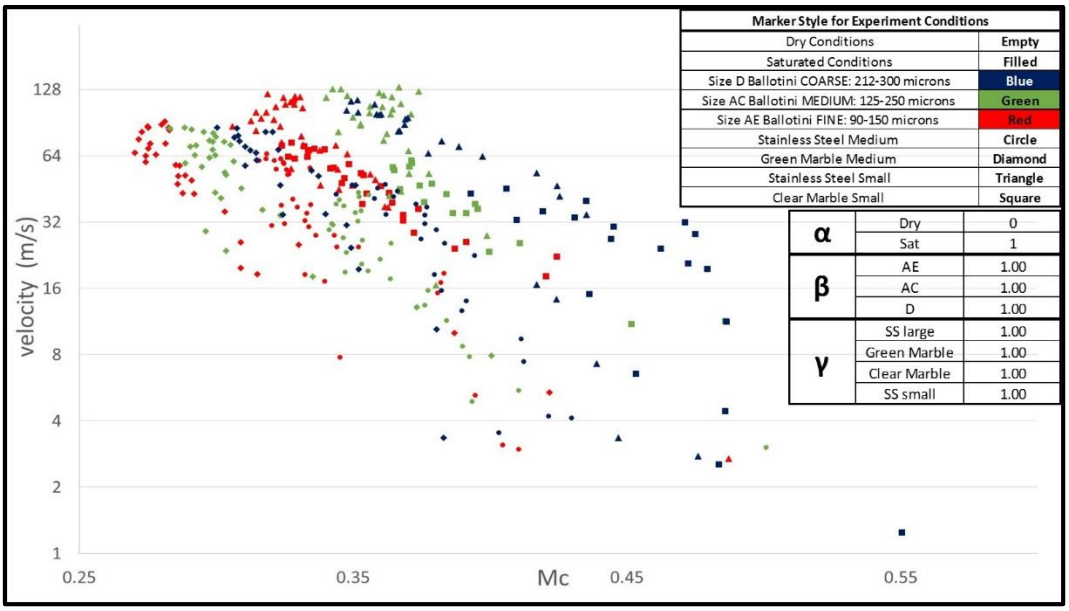

Figure 11- Saturated media shots without any scaling factors.

The above graph (figure 11) shows that initial relationship without scaling. The distinguished differences are first the band separation of grain size distribution, then the separation of impactor density. Figure 12 incorporates the scaling factor for impactor density and shows how the data collapse showing the band separation of grain size.

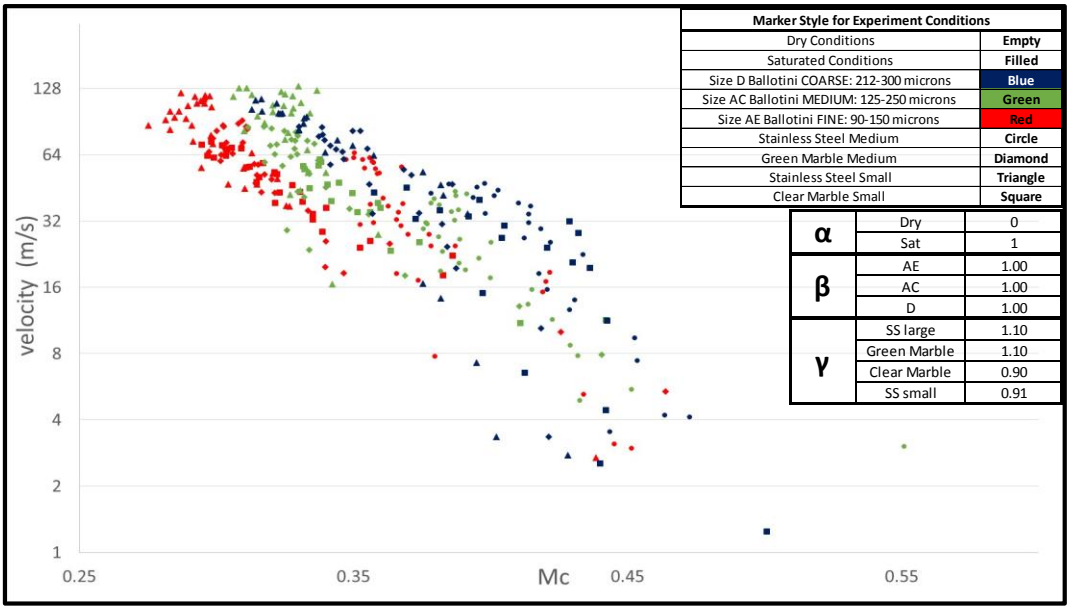

Figure 12- Saturated impact data with γ applied

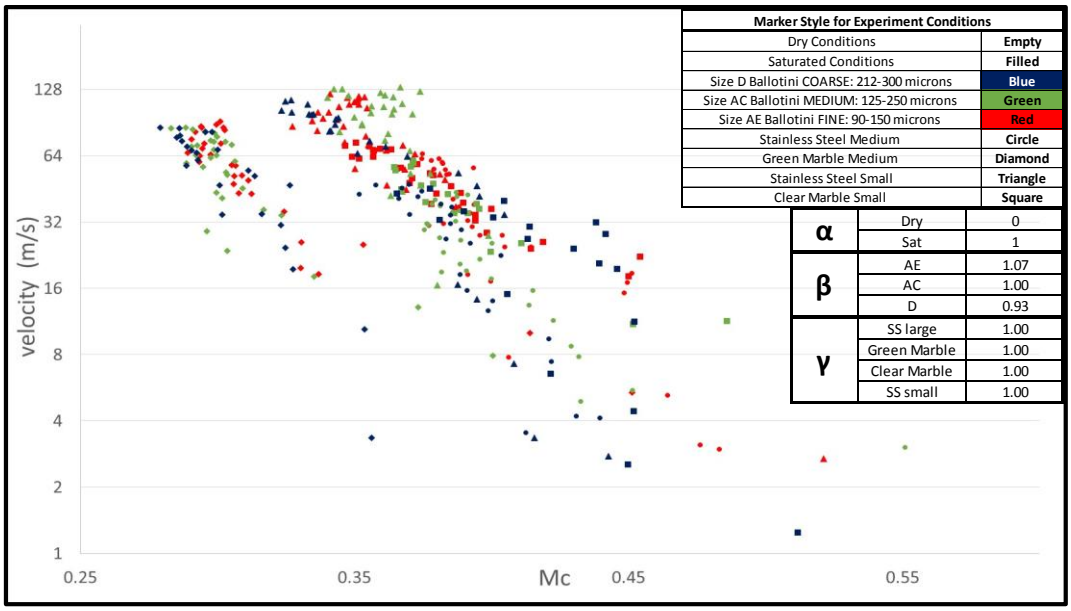

Figure 13- Saturated impact data with β applied

The next step is to show how the data changes with just the implementation of the scaling factor for grain size (figure 13). In this instance the data separates into two bands, one for the stainless steel impactors which are higher density, and one for the lower density glass impactors.

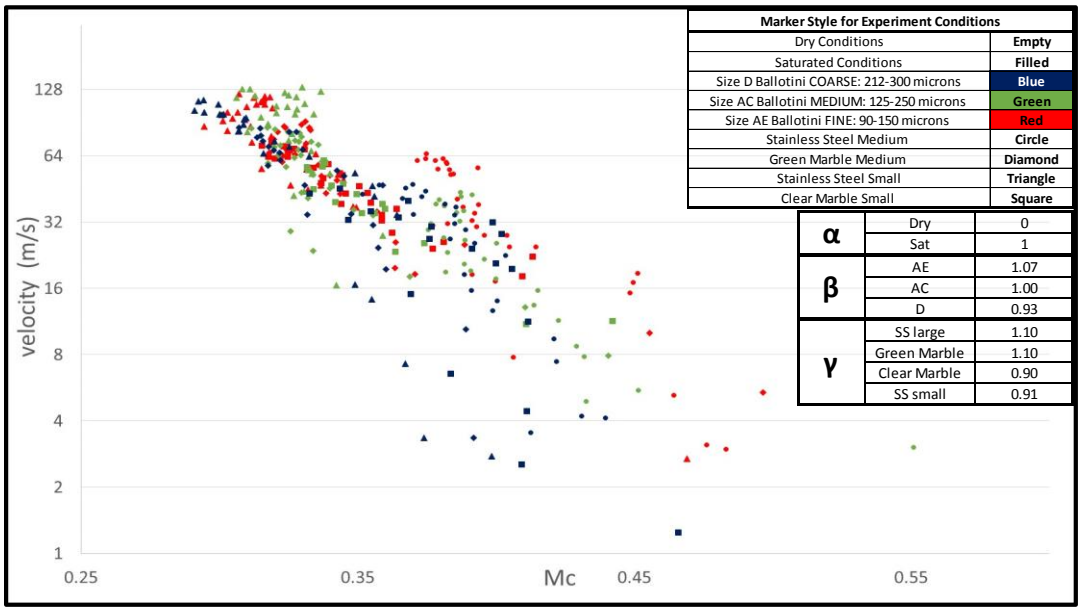

Figure 14-Fully scaled saturated impact data set

The last two figures, 14 and 15, incorporate the scaling factor for both the grain size as well as the impactor densities. We establish an ideal fit for the data and the next step for future work would be to apply information found from the field to this data set and determine if the calculate velocities we find are within the parameters for an impactor. Figure 15 also has the addition of the dry impact data to show that the two sets do not coincide and therefore in order to form a sag like layer the substrate must indeed be saturated.

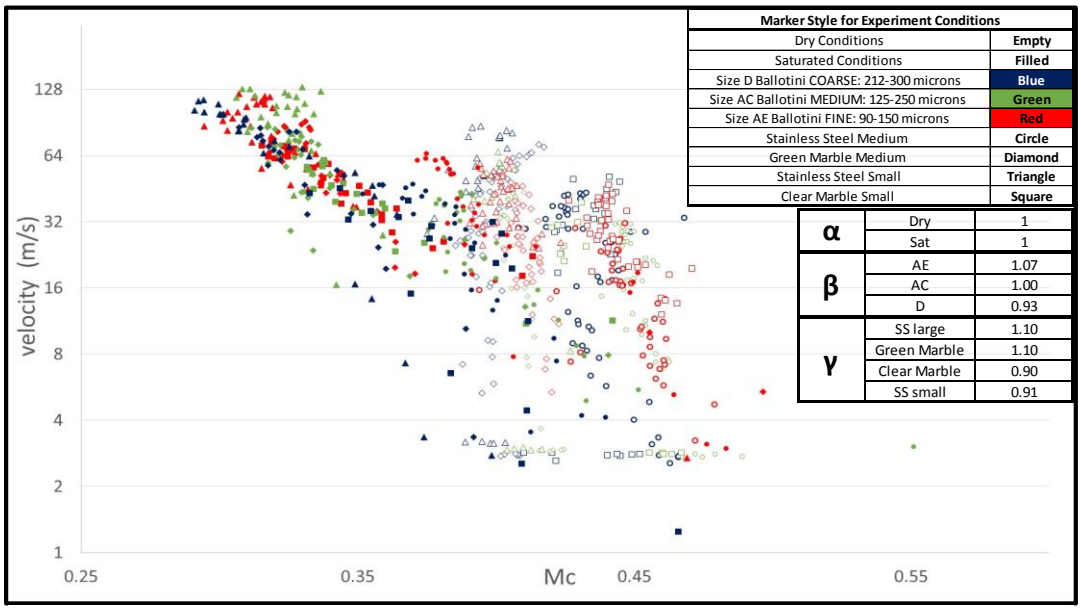

Figure 15-Fully scaled saturated impact data set with the addition of the dry impact data

2.5 Discussion

The morphology of the impact site is determined by a number of factors measured in this study. Oversaturation induces crater filling and erosion by the fluid, thus inhibiting the formation of sedimented sag layers. Upon impact in oversaturated conditions, the impactor will continue to penetrate the underlying strata, even after the total loss of impact energy, because of the added fluidization of the grains from water.

On average the crater diameters of dry substrate impacts are 2.95 times larger than those of impacts into saturated grain beds. This is contributed to the greater cohesion of

grains and lower angle of repose of the wet substrate in relation to that of the dry substrate. This feature is observed in natural cases across many phreatic maars. A dry impact creates a larger volume of ejecta which is shown in the results as well as observations made during experiments.

The average depth of penetration of the saturated impacts is 80.6% of the depth of the dry impacts. The increase in substrate density rapidly halts the kinetic energy of impact. Two factors lead to greater depth of penetration, with one superseding the other. The leading factor for greater penetration depth is impactor density with larger impactor size following. Our data follows this trend aside from an inversion in the finest substrate of the small and medium size stainless steel impactor.

A final comparison was made from previous works from Birch et al 2014 who used a larger variety of impactors at lower velocities. The data sets were fit to equations 2 and 3. These equations include the same variables as equation 1 with the addition of impact velocity (U_i), tangent of angle of repose of the substrate, and two unit less scaling parameters (C and α). The values used for the scaling parameters for this study are shown in table 5. Here, we used a smaller variety of impactors at a larger range of impact velocity. We found that our best fit lines converge at higher energies rather than remain parallel as shown in the previous study (figures 16 and 17).

$$\frac{d}{2R_i} = C_1 \left[\left(\frac{\rho_i}{\rho_s \mu^2} \right)^{\frac{3}{2}} \left(\frac{U_i^2}{2R_i g} \right) \right]^{\alpha_1} \quad \text{(Eq 2)}$$

$$\frac{d}{2R_i} = C_2 \left[\left(\frac{\rho_i}{\rho_s} \right) \left(\frac{U_i^2}{2R_i g} \right) \left(\frac{\delta}{R_i} \right) \right]^{\alpha_1} \quad \text{(Eq 3)}$$

Table 5-Scaling factors for Birch Model

From Birch et al.			
C_1_coarse	0.035	α_1_coarse	0.33
C_1_medium	0.046	α_1_medium	0.33
C_1_fine	0.056	α_1_fine	0.33
C_2_coarse	0.392	α_2_coarse	0.33
C_2_medium	0.415	α_2_medium	0.33
C_2_fine	0.482	α_2_fine	0.33
From this study			
C_1_coarse	0.067	α_1_coarse	0.33
C_1_medium	0.024	α_1_medium	0.41
C_1_fine	0.007	α_1_fine	0.49
C_2_coarse	0.528	α_2_coarse	0.28
C_2_medium	0.455	α_2_medium	0.34
C_2_fine	0.232	α_2_fine	0.43

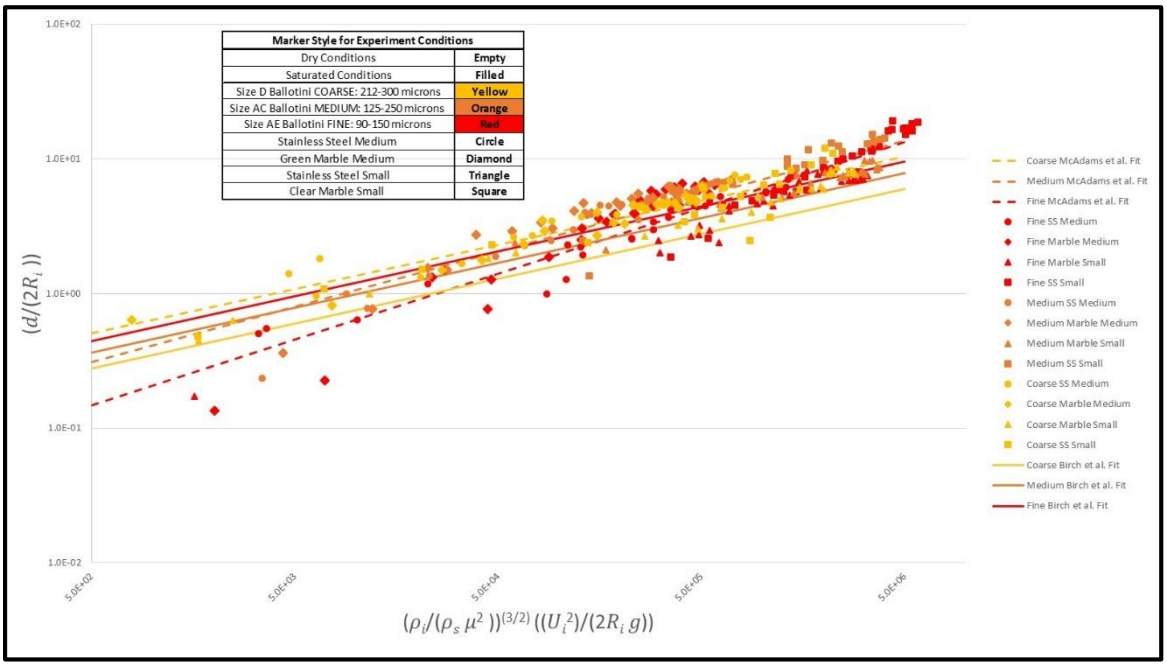

Figure 16- Model using tangent of angle of repose of the substrate (μ)

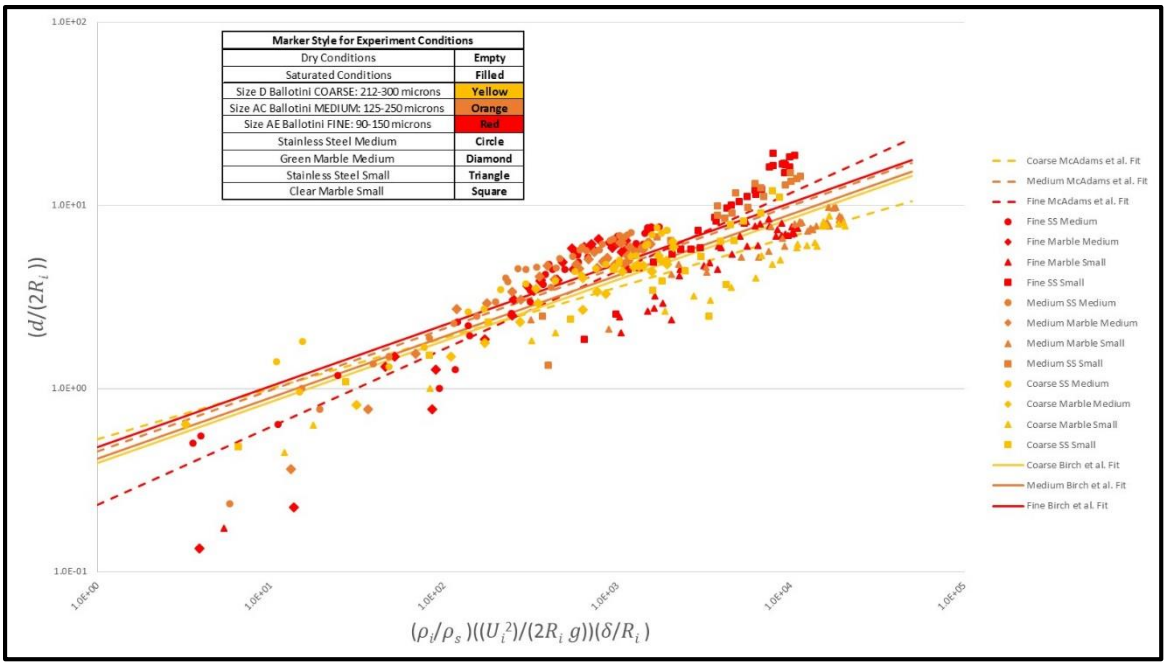

Figure 17- Model using average grain size of the substrate (δ)

CHAPTER 3. FUTURE WORK

3.1 Goals in future work

Using a specifically designed rheometer cup we plan to characterize the rheology of the grains in saturated and dry conditions (figure 18). The information given from a rheometer is of greater validity than that of previous methods. For the current work in order to obtain angle of repose for dry media the grains were poured into a mound and then the angle was measured using image processing (figure 19). The angle of repose for saturated media cannot be established by this method, for this work an angle of repose from the literature was used (Webster et al., 1919). Once a valid angle of repose for the saturated glass media is established we will incorporate the values into both the Birch model as well as the McAdams model.

The next goal is to fit real world data to McAdams et al. model using the data from bomb sag out crop photos from Mendez et al. (in prep). Using a large, 10-20 millimeters in diameter, glass marble impactor we plan to create a cross section of a saturated impact at close to terminal velocity (within 10%). By using colored glass beads in layers within the substrate we will preserve the bomb-sag profile by freezing the grain bed post impact.

Figure 18-Rheometer cup with angled and flat inserts

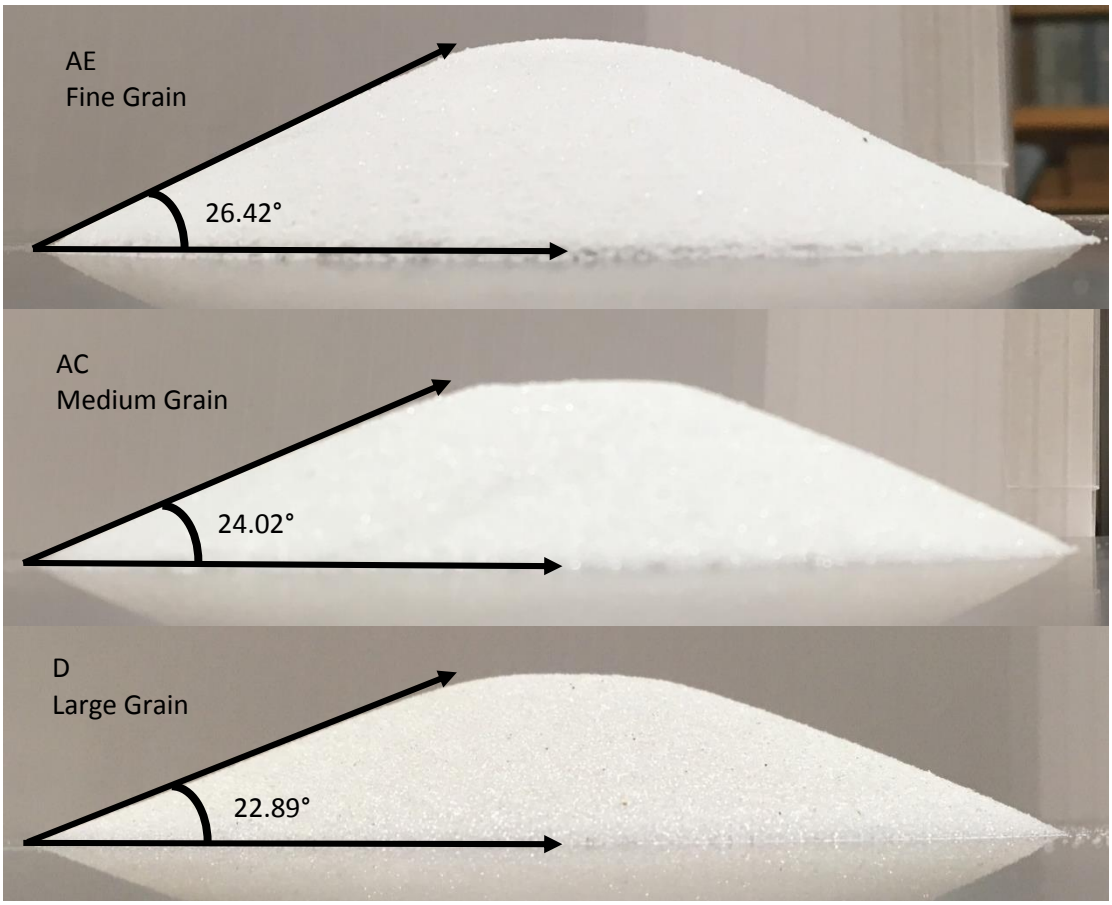

Figure 19- Angle of repose of dry substrate

APPENDIX RAW DATA

Table 6

Saturated substrate	Solid circle markers with solid line
Dry substrate	Hollow diamond markers with dotted line
Medium Stainless Steel Sphere	Blue
Small Stainless Steel Sphere	Grey
Medium Marble Sphere	Orange
Small Marble Sphere	Green

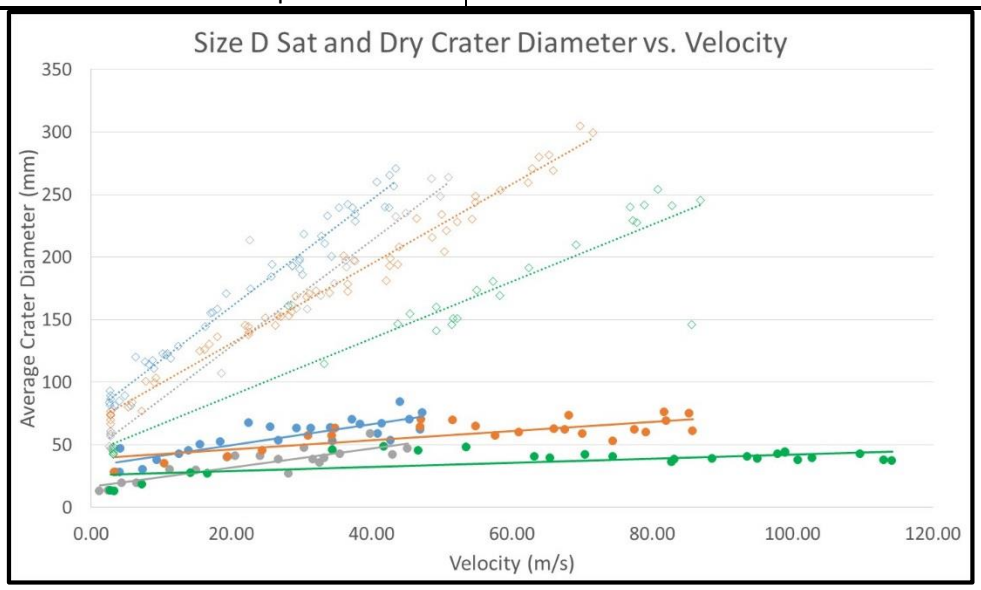

Figure 20

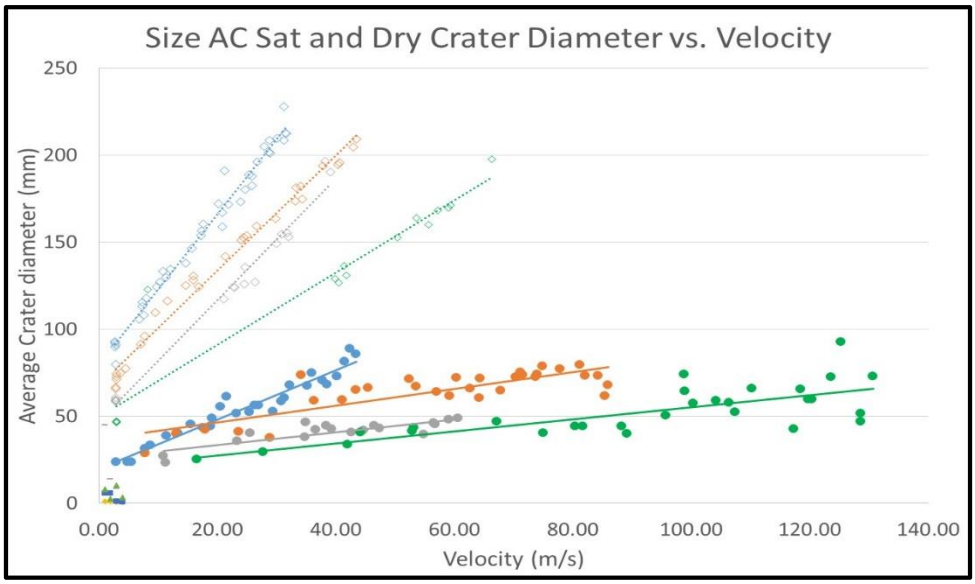

Figure 21

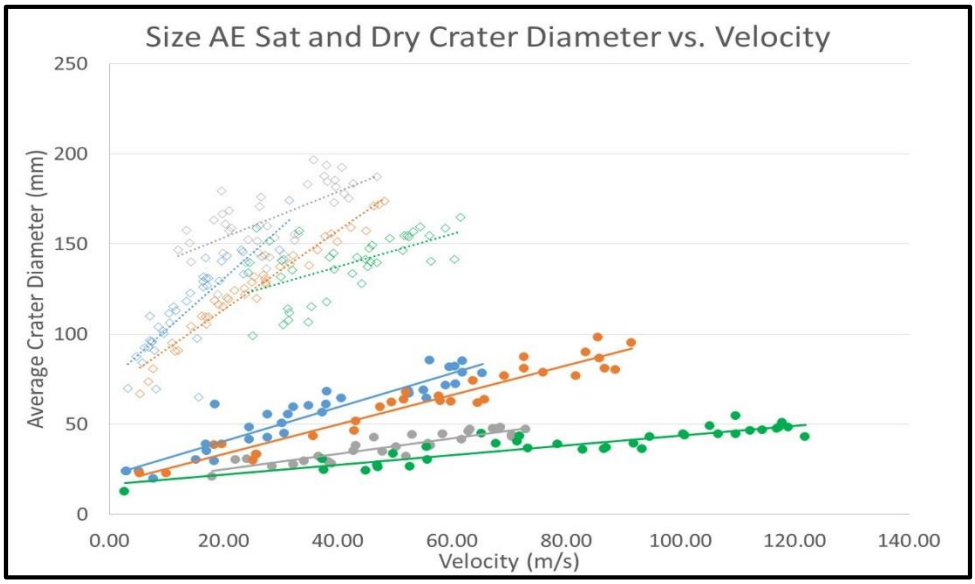

Figure 22

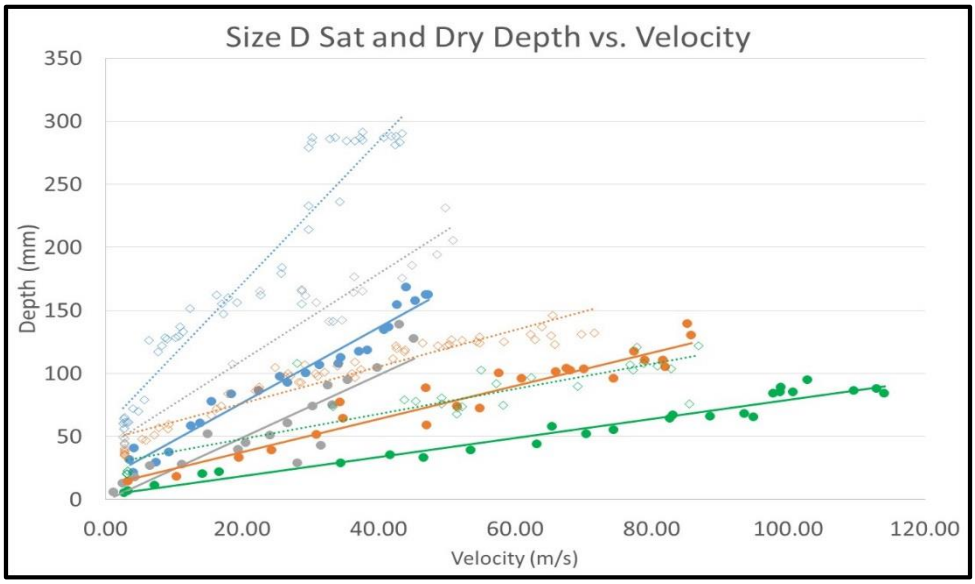

Figure 23

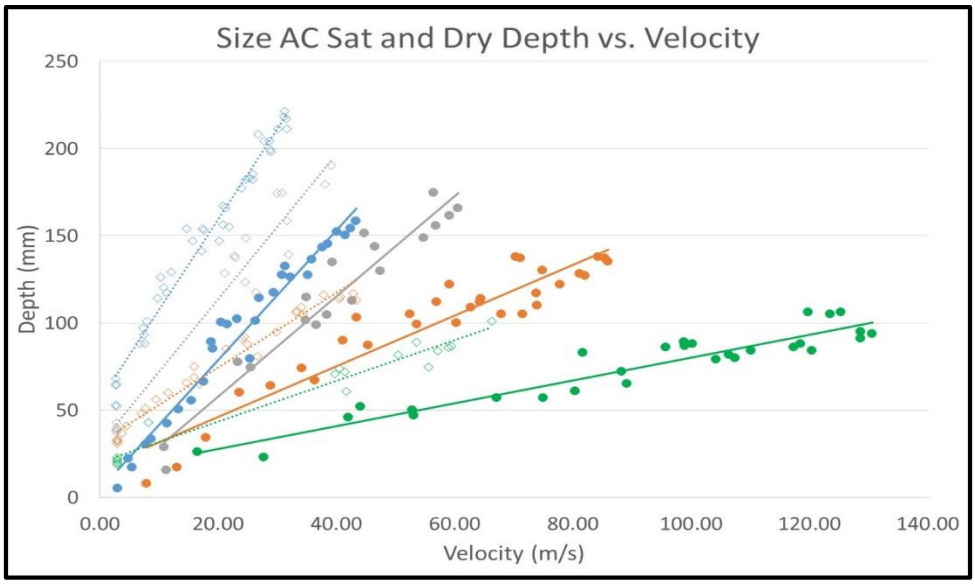

Figure 24

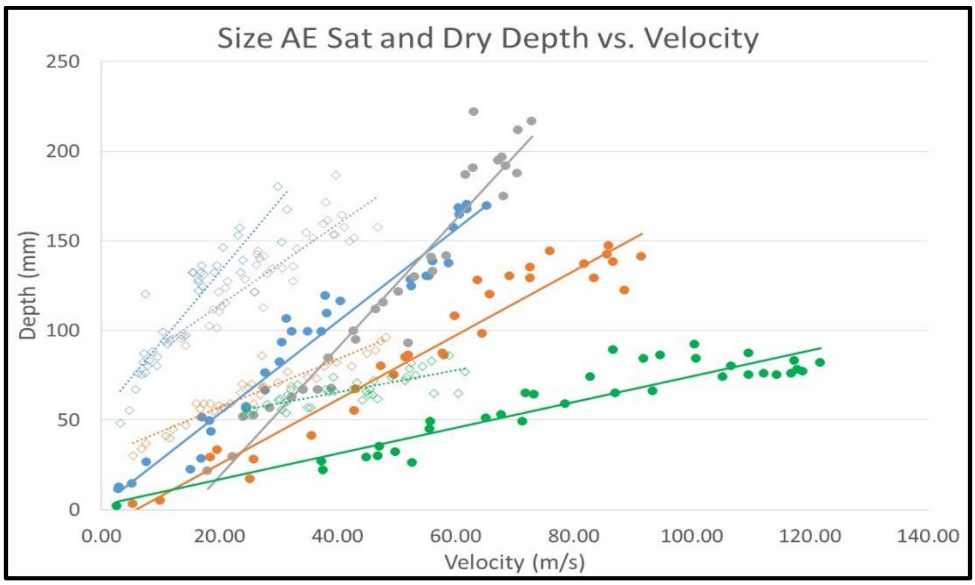

Figure 25

REFERENCES

Birch, S. P. D., et al. "Penetration of spherical projectiles into wet granular media." Physical Review E 90.3 (2014): 032208.

Bower, Sally M., and Andrew W. Woods. "On the dispersal of clasts from volcanic craters during small explosive eruptions." Journal of Volcanology and Geothermal Research 73.1-2 (1996): 19-32.

Brzinski III, Theodore A., et al. "Penetration depth scaling for impact into wet granular packings." Physical Review E 91.2 (2015): 022202.

Brown, Sarah K., et al. "Volcanic fatalities database: analysis of volcanic threat with distance and victim classification." Journal of Applied Volcanology 6.1 (2017): 15.

Calder, E. S., et al. "Mobility of pyroclastic flows and surges at the Soufriere Hills Volcano, Montserrat." Geophysical Research Letters 26.5 (1999): 537-540.

Carey, Steven, and R. S. J. Sparks. "Quantitative models of the fallout and dispersal of tephra from volcanic eruption columns." Bulletin of Volcanology 48.2 (1986): 109-125.

Carrasco-Núñez, Gerardo, Michael H. Ort, and Claudia Romero. "Evolution and hydrological conditions of a maar volcano (Atexcac crater, Eastern Mexico)." Journal of Volcanology and Geothermal Research 159.1 (2007): 179-197.

Clark, Abram H., Lou Kondic, and Robert P. Behringer. "Particle scale dynamics in Granular impact." Physical review letters 109.23 (2012): 238302.

Francis, P. W. "Cannonball bombs, a new kind of volcanic bomb from the Pacaya volcano, Guatemala." Geological Society of America Bulletin 84.8 (1973): 2791-2794.

Isola, Riccardo. Packing of granular materials. University of Nottingham, 2008.

Katsuragi, Hiroaki, and Douglas J. Durian. "Unified force law for granular impact cratering." Nature Physics 3.6 (2007): 420-423.

Manga, Michael, et al. "Wet surface and dense atmosphere on early Mars suggested by the bomb sag at Home Plate, Mars." Geophysical Research Letters 39.1 (2012).

Mastin, Larry G. A simple calculator of ballistic trajectories for blocks ejected during volcanic eruptions. No. 2001-45. US Geological Survey, 2001.

Morrison, Faith A. "Data correlation for drag coefficient for sphere." Department of Chemical Engineering, Michigan Technological University, Houghton, MI (2013).

Schmid, R. "Descriptive nomenclature and classification of pyroclastic deposits and fragments: Recommendations of the IUGS Subcommission on the Systematics of Igneous Rocks." Geology 9.1 (1981): 41-43.

Scott, W. E., and R. G. McGimsey. "Mass, distribution, grain size, and origin of 1989-1990 tephra-fall deposits of Redoubt Volcano, Alaska."

Sparks, R. S. J., and L. Wilson. "Explosive volcanic eruptions—V. Observations of plume dynamics during the 1979 Soufrière eruption, St Vincent." Geophysical Journal International 69.2 (1982): 551-570.Steinburg

Taddeucci, J., et al. "In-flight dynamics of Volcanic Ballistic Projectiles." Reviews of Geophysics (2017).

Walker, G. PL, and R. Croasdale. "Characteristics of some basaltic pyroclastics." Bulletin of Volcanology 35.2 (1971): 303-317.
Walker, G. P. L., and R. Croasdale. "Characteristics of some basaltic pyroclastics." Bulletin volcanologique 35.2 (1971): 303-317.
Webster, Arthur Gordon. "On the angle of repose of wet sand." Proceedings of the National Academy of Sciences of the United States of America (1919): 263-265.
Wilson, L., and G. P. L. Walker. "Explosive volcanic eruptions-VI. Ejecta dispersal in plinian eruptions: the control of eruption conditions and atmospheric properties." Geophysical Journal International 89.2 (1987): 657-679.
"The Drag Equation." NASA. NASA Glenn Research Venter, 05 May 2015. Web. 19 Apr. 2017.